

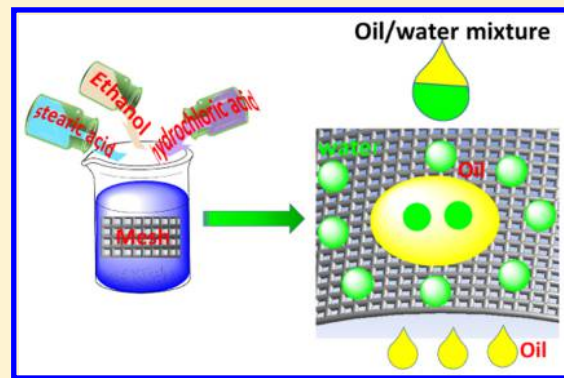
# Simple and Green Fabrication of a Superhydrophobic Surface by One-Step Immersion for Continuous Oil/Water Separation

Jingfang Zhu,<sup>†,‡</sup> Bin Liu,<sup>†</sup> Longyang Li,<sup>‡</sup> Zhixiang Zeng,<sup>\*,‡</sup> Wenjie Zhao,<sup>\*,‡</sup> Gang Wang,<sup>‡</sup> and Xiaoyan Guan<sup>‡</sup>

<sup>†</sup>School of Materials Science and Engineering, North University of China, Taiyuan 030051, People's Republic of China

<sup>\*</sup>Key Laboratory of Marine Materials and Related Technologies, Zhejiang Key Laboratory of Marine Materials and Protective Technologies, Ningbo Institute of Materials Technology and Engineering, Chinese Academy of Sciences, Ningbo 315201, People's Republic of China

**ABSTRACT:** In this paper, stainless steel meshes with superhydrophobic and superoleophilic surfaces were fabricated by rapid and simple one-step immersion in a solution containing hydrochloric acid and stearic acid. The apparent contact angles were tested by a video contact angle measurement system (CA). Field emission scanning electron microscopy (FE-SEM), Fourier transform infrared spectroscopy (FTIR), and X-ray photoelectron spectroscopy (XPS) were conducted to characterize the surface topographies and chemical compositions. The SEM results showed that mesh surfaces were covered by ferric stearate ( $\text{Fe}[\text{CH}_3(\text{CH}_2)_{16}\text{COO}]_2$ ) with low surface energy. The CA test results showed that the mesh had a maximum apparent contact angle of  $160 \pm 1.0^\circ$  and a sliding angle of less than  $5.0^\circ$  for the water droplet, whereas the apparent contact angle for the oil droplet was zero. Ultrasound oscillation and exposure tests at atmospheric conditions and immersion tests in 3.5 wt % NaCl aqueous solution were conducted to confirm the mesh with excellent superhydrophobic and superoleophilic properties. On the basis of the superhydrophobic mesh, a miniature separation device pump was designed to collect pure oil from the oil/water mixture. It showed that the device was easier and convenient. The techniques and materials presented in this work are promising for application to wastewater and oil spill treatment.



## 1. INTRODUCTION

With the development of industry, humans confront increasing issues about crude oil leakage accidents, industrial sewage discharge, and oily water.<sup>1–3</sup> According to statistics, millions of tons of crude oil and refined oil leak into the sea every year,<sup>4</sup> which has caused severe damage to the marine ecosystem. Furthermore, the oil also causes serious harm to human health through the food chain, indirectly.<sup>5–7</sup> Hence, effective treatment of oily water has become a hotspot in the research field of environmental protection.<sup>8,9</sup>

Traditionally, oily water treatment techniques include dissolved air flotation, centrifugation methods, absorbents, chemical dispersants, adsorption bioremediation, gravity separation, solidifiers, in situ burning, and so forth.<sup>8,10–15</sup> These techniques still show some limitations in practical application, such as low efficiency, being time-consuming, allowing for recontamination, and having high operation costs.<sup>15</sup> Therefore, researchers have paid more attention to the development of superhydrophobic materials for the treatment of oily water due to their highly efficient and environmental benefits.

Recently, materials with superhydrophobicity and superoleophilicity<sup>8,16,17</sup> have been investigated for highly effective oil/water separation, including textiles,<sup>18</sup> metal foam,<sup>19</sup> graphene sponges,<sup>20</sup> polymer and carbon nanotube sponges,<sup>20</sup> polyurethane

sponges,<sup>21</sup> cellulose sponges,<sup>22</sup> silicone sponges,<sup>23</sup> and a range of 3D porous materials.<sup>24–30</sup> However, previous literature mainly concentrated on the oil absorption capacity and disregarded the complex preparation procedure and the inconvenience in application. For example, the synthesis process was time-consuming, and the oil recovery processes often needed dreary mechanical squeezing or distillation, which caused recontamination and high cost.<sup>31</sup> For example, various coated meshes of the biomimetic materials were reported by a number of scientists. Grynyov et al. fabricated omniphobic metallic surfaces by immersing the mesh in a 97% perfluororonanoic acid solution. The omniphobic stainless steel surfaces were covered by the hierarchical micro- and submicro-scaled relief and showed excellent water and oil repellence.<sup>32</sup> Darmanin et al. fabricated superoleophobic surfaces on the stainless steel mesh by electrodeposition of conducting polymer containing short perfluorobutyl chains. The best oleophobicity ( $\theta_{\text{sunflower oil}} = 150^\circ$  and  $\theta_{\text{hexadecane}} = 136^\circ$ ) property was obtained.<sup>33</sup> These materials exhibit high performance for separation of oil/water. Bormashenko et al. fabricated microscaled porous metallic polymer meshes with the breath-figures self-assembly and

designed a novel device to collect and recycle oil without any mechanical squeezing.<sup>34</sup>

In this paper, stainless steel meshes with superhydrophobic and superoleophilic surfaces were synthesized only by immersing into an ethanol solution including HCl and stearic acid. This preparation process is convenient, fast, low-cost, and green, and the obtained materials have promising application for oily water treatment.

## 2. EXPERIMENTAL METHODS

**2.1. Materials.** Reagents were purchased from Aladdin Reagent. The (304) stainless steel mesh samples with an average pore diameter of approximately 100  $\mu\text{m}$  were used as substrates.

**2.2. Sample Preparation.** The detailed fabrication process can be described as follows. The stainless steel mesh substrates

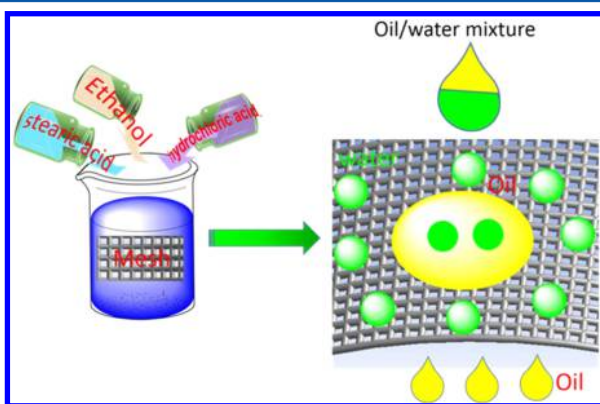


Figure 1. Schematic of the fabrication process of superhydrophobic stainless steel mesh and application to oil/water separation.

were cleaned by water and then successively ultrasonically washed in a hydrochloric acid (2 mol/L) solution (10 min), acetone (5 min), ethanol (2 min), and deionized (DI) water in order to remove oxidizing material, organic compounds, oil, and other remnant dirt. Finally, the mesh was immersed into ethanol solution containing HCl with the concentration varying from 1 to 8 mol/L and stearic acid  $\text{CH}_3(\text{CH}_2)_{16}\text{COOH}$  with the concentration varying from 0.01 to 0.08 mol/L, for different times and temperatures. Figure 1 shows the fabrication process of superhydrophobic stainless steel mesh and the sketch of oil/water separation.

**2.3. Sample Characterization.** FE-SEM (FEI Quanta 250 FEG, U.S.A.) was used to characterize the surface topographies of samples. A viewgraph model with an oblique angle of 45° was used for all measurements. The chemical compositions of the mesh surfaces were examined by Fourier transform infrared spectroscopy (FTIR), and X-ray photoelectron spectroscopy (XPS). The samples with hydrophobicity and lipophilicity were measured by a video contact angle measurement system (OCA20, Germany) with a water droplet (5.0  $\mu\text{L}$ ) and oil droplet (5.0  $\mu\text{L}$ ), respectively. The apparent contact angle of every mesh sample was measured at least five times, and the obtained average value was used for subsequent data analysis.

## 3. RESULTS AND DISCUSSION

**3.1. Surface Morphology.** Figure 2 shows the SEM images of the original stainless steel mesh surface and stainless steel mesh treated with immersion in an ethanol solution with 4 mol/L HCl and 0.06 mol/L stearic acid, at 80 °C for 60 min. For the original stainless steel meshes, the surface was very smooth and clear, as shown in Figure 2a. Figure 2b–d shows the surface structures of stainless steel meshes with different magnifications after immersion. It can be seen that the stainless

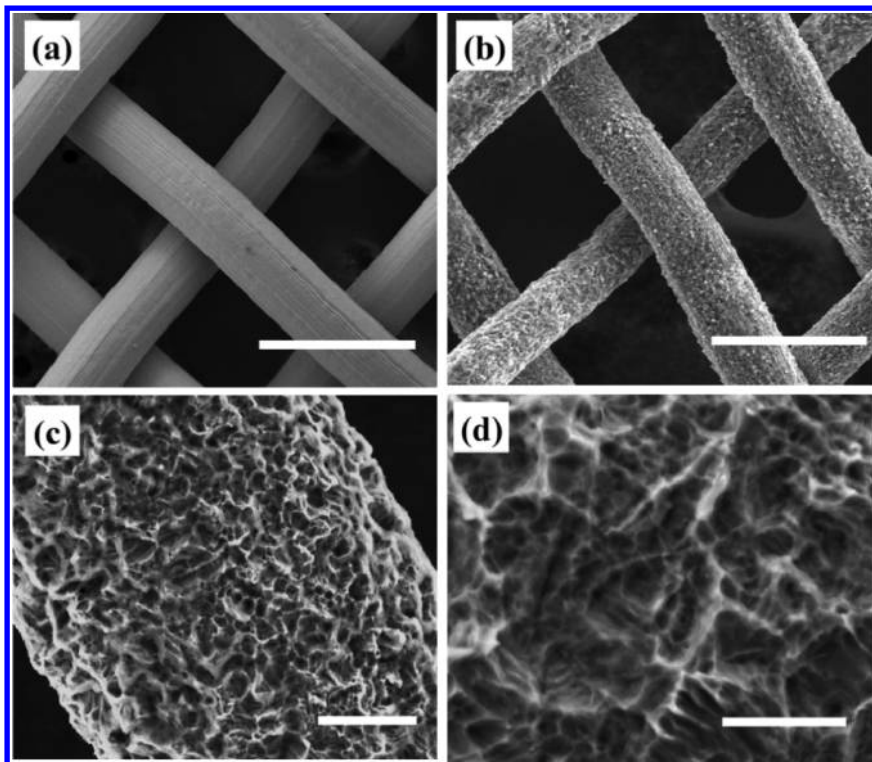


Figure 2. SEM images of the original stainless steel mesh (a) and the obtained mesh with different magnifications (b–d). Scale bars: (a,b) 100, (c) 10, and (d) 1  $\mu\text{m}$ .

steel mesh surface had uniform nanostructures, as shown in Figure 2b,c. In the image with greater magnification (Figure 2d), it seems that the surface was covered by some thin films. The stainless steel samples were etched by chlorine ions and were chemically modified with stearic acid simultaneously, so as to produce the film-covered nanostructure.<sup>35</sup>

In order to confirm the composition of the films, FTIR and XPS were conducted. Figure 3 shows the comparison of FTIR

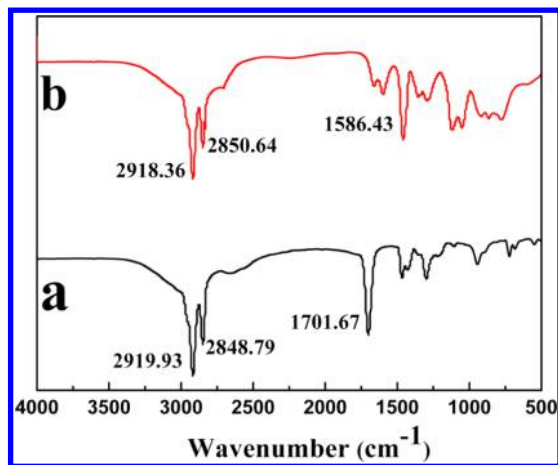


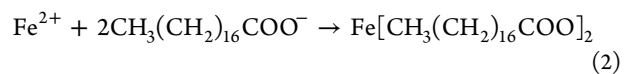
Figure 3. FTIR spectra of stearic acid powder (curve a) and thin films on the mesh surface (curve b).

spectra between stearic acid and the film on mesh. Curve a in Figure 3 shows FTIR spectra of stearic acid. The adsorption peaks at about 2919 and 2848  $\text{cm}^{-1}$  in the high-frequency region are attributed to  $-\text{CH}_2-$  band asymmetric and symmetric stretching vibrations, respectively.<sup>36,37</sup> In the low-frequency region, the peak at 1701  $\text{cm}^{-1}$  is attributed to  $-\text{COOH}$  from

stearic acid. In comparison, from curve b in Figure 3, it can be found that a new adsorption peak appears at 1586.43  $\text{cm}^{-1}$  in the spectrum of the films, while the free  $-\text{COOH}$  band of stearic acid at 1701  $\text{cm}^{-1}$  disappears. The new adsorption peak may be attributed to asymmetric and symmetric stretches of the  $-\text{COO}-$  group. The above analyses show that the stainless steel mesh reacted with stearic acid to form ferric stearate.

XPS was conducted to further confirm the chemical state of the film on the mesh surface. As shown in Figure 4a, the compositions of the mesh film included Fe, C, and O. Figure 4b shows the XPS spectra of Fe 2p. The peaks at binding energies (BE) of 724.6 and 710.8 eV are attributed to the Fe 2p<sub>1/2</sub> and Fe 2p<sub>3/2</sub> of iron compounds, respectively. In Figure 4c, the sharp C 1s peak displays a symmetric spectrum with a weaker intensity shoulder in the higher BE region. The peak at 284.7 eV is attributed to alkyl chain carbon (C-C), and the peak at 288.6 eV is assigned to the carboxyl group (COOH). Figure 4d shows the BE of a single and symmetric O 1s peak at 532.3 eV, revealing the presence of two comparable symmetric O atoms in the carboxylate (COO<sup>-</sup>) group that originated from charge scattering of the carboxylate anion.<sup>38</sup> The above analyses indicate that the immersion process generated ferric stearate on the mesh surface.

The formation mechanism of film-covered nanostructures could be expressed as the following reactions:



**3.2. Influence Factors of Super-Hydrophobicity.** The effects of concentration, time, and temperature on superhydrophobicity were studied. Figure 5a shows the effect of the stearic acid solution on the apparent contact angle. When the

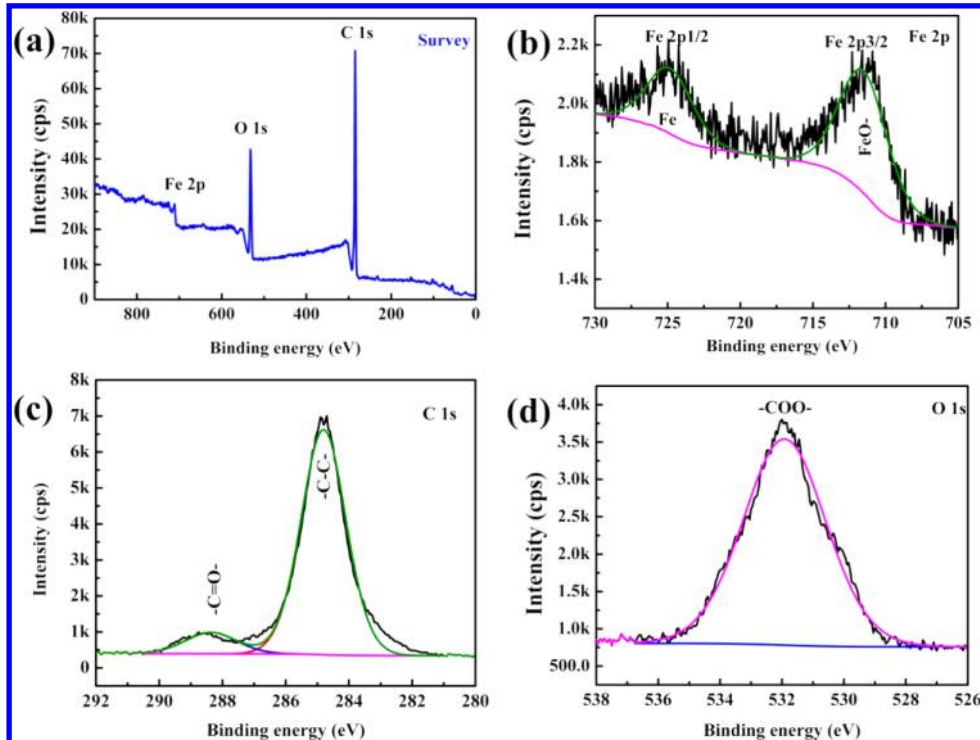
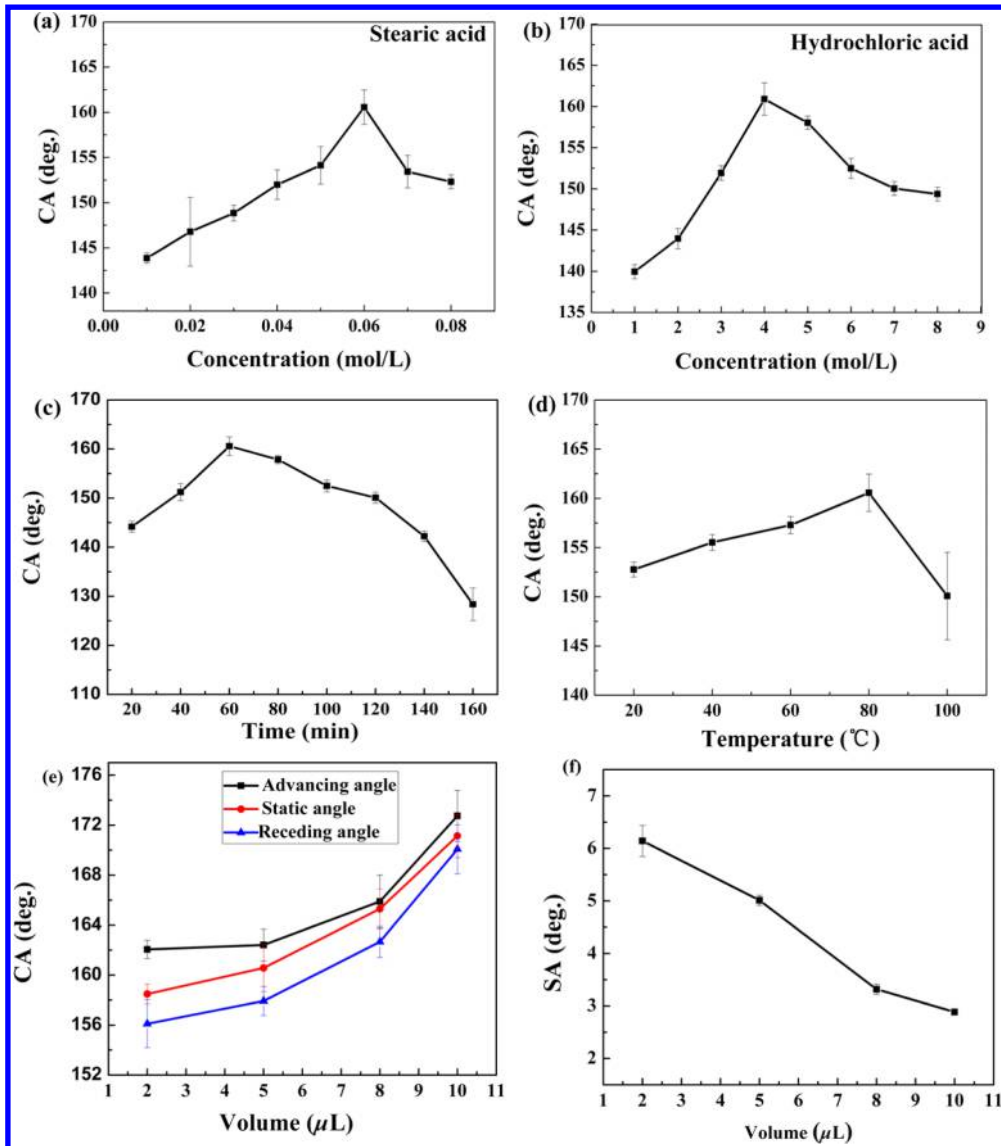


Figure 4. XPS spectra of films on stainless steel mesh after immersion. Survey scan spectra (a) and high-resolution XPS spectra of Fe 2p (b), C 1s (c), and O 1s (d).



**Figure 5.** Apparent contact angle variation with the change of stearic acid solution concentration (a), HCl solution concentration (b), time (c), and temperature (d). The variation of the apparent contact angle, advancing contact angle, and receding contact angle for different droplet volumes (e). The mesh sliding angle depending on the droplet volume (f).

HCl concentration was kept at 4 mol/L, the apparent contact angles increased from  $143 \pm 1.0$  to  $160 \pm 1.0^\circ$  with increasing concentrations of stearic acid in the range from 0.01 to 0.06 mol/L. However, the apparent contact angles began to decrease when the stearic acid concentrations continued to increase, at 80 °C for 60 min.

Figure 5b shows the effect of HCl solution on the apparent contact angles. When the stearic acid concentration was kept to 0.06 mol/L, the apparent contact angles increased from  $145 \pm 1.0$  to  $160 \pm 1.0^\circ$  with increasing concentrations of HCl in the range from 1 to 4 mol/L. However, the apparent contact angles began to decrease to  $149 \pm 1.0^\circ$  when the HCl concentrations continued to increase, at 80 °C for 60 min.

Figure 5c shows the influence of immersion time on the apparent contact angle when the conditions were kept at 0.06 mol/L stearic acid, 4 mol/L HCl, and 80 °C. It can be seen that when the time was prolonged from 20 to 60 min, the apparent contact angles increased from  $145 \pm 0.7$  to  $160 \pm 1.0^\circ$ . As time continued to increase from 60 to 160 min, the apparent contact angles decreased.

The immersion temperature exhibited an important influence on the apparent contact angle, as shown in Figure 5d. With 0.06 mol/L stearic acid, 4 mol/L HCl, and an immersion time of 60 min, the apparent contact angle increased from  $152 \pm 1.0$  to  $160 \pm 1.0^\circ$  with the temperature increasing from 20 to 80 °C. Then contact angle decreased to  $150 \pm 0.8^\circ$  when the temperature reached 100 °C.

The above results indicate that the proper stearic acid and HCl concentrations, temperature, and immersion time could result in excellent superhydrophobicity for mesh. With 0.06 mol/L stearic acid, 4 mol/L HCl, a temperature of 80 °C, and an immersion time of 60 min, the obtained mesh exhibited uniform nanostructures and an apparent contact angle of  $160 \pm 1.0^\circ$ . Excessive stearic acid led to the decrease of the apparent contact angle because excessive ferric stearate would cover the nanostructures. Excessive HCl and immersion time and high temperature would result in excessive corrosion of the metal mesh and damage the nanostructures.

The relationship between the droplet volume and wetting ability for the mesh surfaces was investigated, as shown in

Figure 5e. Droplets with volumes of 2, 5, 8, and 10  $\mu\text{L}$  were used. The notion of contact angle hysteresis was equal to the difference value between advancing and receding contact angles. It was found that the contact angle hysteresis of the droplet was in the range of 2.6–6.0°, as shown in Figure 5e. With the increase of droplet volume, the droplet shape became oblate due to gravity. Therefore, the apparent contact angle increased and the sliding angle decreased with the increase of droplet volume (Figure 5e,f).

### 3.3. Dynamic Wetting Behavior of the Oil and Water.

Figure 6a shows the contact deformation and departure process

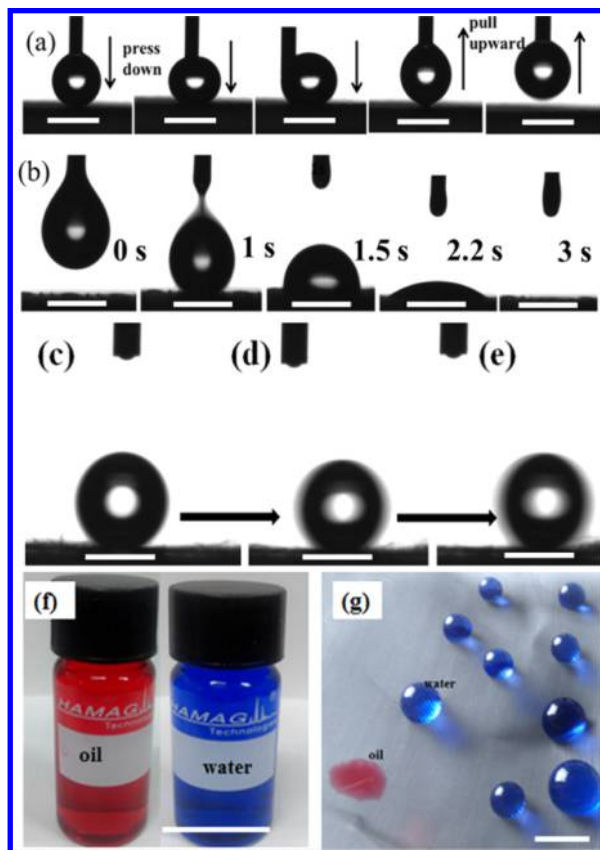


**Figure 6.** Dynamic contact and departure process for the water droplet (5  $\mu\text{L}$ ) (a). The arrows show the moving direction of the water droplet. Photographs of dynamic measurements of oil wettability for the obtained mesh (b). The sliding process for the water droplet (5  $\mu\text{L}$ ) on the obtained mesh (c–e). Image of dyed oil and dyed water (f). Many ball-like water droplets were uniformly distributed on the obtained mesh (g). Scale bars: (a–e) 2, (f) 25, and (g) 5 mm.

of the water droplet (5  $\mu\text{L}$ ) on the superhydrophobic surface. It suggests that the obtained mesh shows excellent superhydrophobicity and low adhesion properties. In Figure 6a, it is clearly observed that the water droplet can completely detach from the stainless steel mesh and nonwet the mesh surface even after press and deformation.

The wettability of the oil permeation on the obtained mesh surface was investigated by the apparent contact angle measurement, as shown in Figure 6b. A peanut oil droplet (5  $\mu\text{L}$ ) was used to evaluate the oil wettability, and the apparent contact angle quickly became zero in 3 s after the peanut oil contacted the surface. However, the water droplet (5  $\mu\text{L}$ ) easily rolled after 120 ms, as shown in Figure 6c,e. It indicates that the mesh surface exhibited low water adhesion and high oil adhesion.

The digital images (Figure 6f,g) show the states of water droplets (colored by methyl blue) and peanut oil (colored by Sudan red) on the mesh.

Many blue ball-like water droplets were distributed on the stainless steel mesh surface, indicating the uniform property of the stainless steel mesh surface. In contrast, peanut oil immediately penetrated into the mesh. It indicated that the obtained mesh had prominent superhydrophobicity and superoleophilicity.

**3.4. Stability of the Obtained Mesh and Its Application for Oil/Water Separation.** The mesh with pore sizes of 100  $\mu\text{m}$  exhibited the best superhydrophobicity, as shown in Figure 7a. When the mesh pore size was below 100  $\mu\text{m}$ , the apparent contact angle decreased due to the decreased air–water interface. However, when the mesh pore size was higher than 100  $\mu\text{m}$ , the mesh pore size was too large to store the air in the structure, so the surface tension could hold the water droplet. As the mesh pore size continued to increase, the superhydrophobic performance of the mesh decreased. Therefore, the ideal pore size for the mesh is 100  $\mu\text{m}$ . The obtained mesh with a 100  $\mu\text{m}$  pore size was folded into a small box (4  $\times$  3  $\times$  1  $\text{cm}^3$ ), as shown in Figure 7b. The small box could freely float on the water because of its superhydrophobicity. The oil rapidly permeated into the box while water was completely rejected.

The stability of the superhydrophobic mesh surface was evaluated via testing the apparent contact angle before and after ultrasonic oscillation. The apparent contact angle of the obtained mesh for the water droplet (5  $\mu\text{L}$ ) was  $160 \pm 1.0^\circ$  before ultrasonic oscillation and was  $158 \pm 1.3^\circ$  after ultrasonic oscillation, as shown in Figure 7c,d. The change of apparent contact angles was nearly negligible. The obtained mesh was exposed to the atmosphere for 60 days, and the mesh surface with superhydrophobicity was stable, as shown in Figure 7e. Further, the mesh was immersed in a 3.5 wt % NaCl aqueous solution for 12 days. It was found that the apparent contact angle of the obtained mesh for the water droplet (5  $\mu\text{L}$ ) was kept almost stable, as shown in Figure 7f.

On the basis of the obtained mesh, a miniature apparatus was designed for oil/water separation, as shown in Figure 8. When turning on the self-priming pump, it can be seen that only pure oil (peanut oil, diesel oil, and gasoline) penetrated the mesh and dropped into the container, while water successfully passed through the mesh. Obviously, it can continuously collect pure oil from the oil/water mixture.

## 4. CONCLUSIONS

Stainless steel mesh surfaces with uniform nanostructures and extremely low surface energy were fabricated via immersion in the solution containing HCl and stearic acid. They showed superhydrophobic and superoleophilic properties. Under optimum conditions, the obtained mesh exhibited an apparent contact angle of  $160 \pm 1.0^\circ$  for the water droplet and  $0^\circ$  for the oil droplet. The superhydrophobic samples were stable by ultrasonic oscillation, exposure tests in the atmosphere, and immersion corrosion tests in a 3.5 wt % NaCl aqueous solution. On the basis of the obtained mesh, a miniature oil/water separation device was designed, which could be simply and effectively used for the separation of an oil/water mixture. The method in this study is suitable for larger-scale fabrication and has potential applications in oil/water separation.

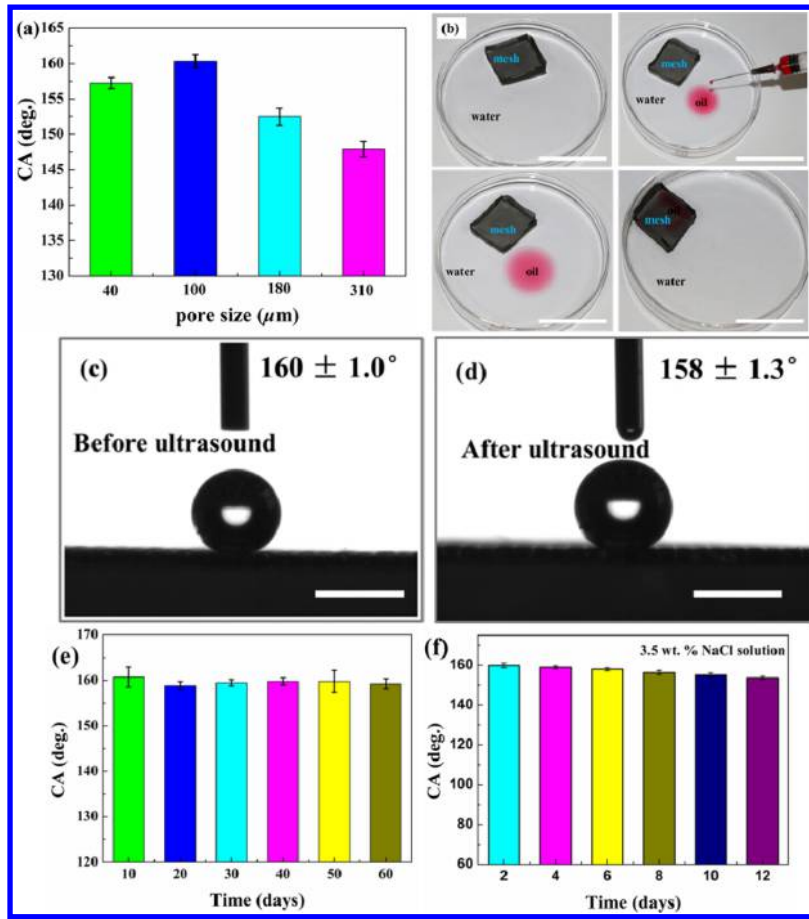


**Figure 7.** Effect of pore size on the apparent contact angle (a). Collection process of peanut oil on the water surface by the mesh box (b). Apparent contact angle before ultrasound oscillation (c) and after ultrasound oscillation (d) in water. Apparent contact angle for the mesh exposure to air at room temperature (e). Apparent contact angle for mesh after corrosion in a 3.5 wt % NaCl aqueous solution (f). Scale bars: (b) 40 and (c,d) 2 mm.

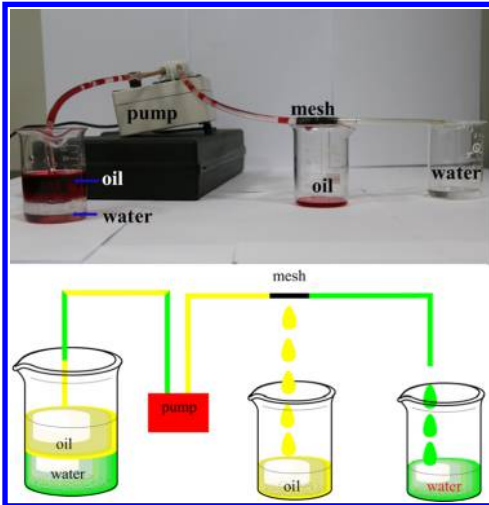


**Figure 8.** Photograph of the experimental apparatus continuously collecting pure oil from the oil/water mixture and schematic diagram of the oil/water separation apparatus.

## AUTHOR INFORMATION

### Corresponding Authors

\*E-mail: [zengzhx@nimte.ac.cn](mailto:zengzhx@nimte.ac.cn). Phone: 0574-86685809.

\*E-mail: [zhaowj@nimte.ac.cn](mailto:zhaowj@nimte.ac.cn). Phone: 0574-86694901.

### Notes

The authors declare no competing financial interest.

## ACKNOWLEDGMENTS

We express our sincere gratitude to the National Basic Research Program of China (No. 2014CB643302), the National Nature Science Foundation of China (No. 51475450 and 51335010), the Zhejiang Provincial Innovation Team (No. 2011R50006), and the Ningbo Municipal Innovation Team (No. 2011B81001).

## REFERENCES

- Chu, Z.; Feng, Y.; Seeger, S. Oil/water separation with selective superantiwetting/superwetting surface materials. *Angew. Chem., Int. Ed.* **2015**, *54*, 2328–2338.
- Jayaramulu, K.; Datta, K. K.; Rosler, C.; Petr, M.; Otyepka, M.; Zboril, R.; Fischer, R. A. Biomimetic superhydrophobic/superoleophilic highly fluorinated graphene oxide and zif-8 composites for oil/water separation. *Angew. Chem., Int. Ed.* **2016**, *55*, 1178–1182.
- Zhu, L.; Chen, M.; Dong, Y.; Tang, C. Y.; Huang, A.; Li, L. A low-cost mullite-titania composite ceramic hollow fiber microfiltration membrane for highly efficient separation of oil/in-water emulsion. *Water Res.* **2016**, *90*, 277–285.
- Ma, Q.; Cheng, H.; Fane, A. G.; Wang, R.; Zhang, H. Recent development of advanced materials with special wettability for selective oil/water separation. *Small* **2016**, *12*, 2186–2202.
- Wan, Y.; Wang, B.; Khim, J. S.; Hong, S.; Shim, W. J.; Hu, J. Naphthenic acids in coastal sediments after the Hebei Spirit oil spill: A potential indicator for oil contamination. *Environ. Sci. Technol.* **2014**, *48*, 4153–4162.
- Zhang, W.; Shi, Z.; Zhang, F.; Liu, X.; Jin, J.; Jiang, L. Superhydrophobic and superoleophilic PVDF membranes for effective

separation of water-in-oil emulsions with high flux. *Adv. Mater.* **2013**, *25*, 2071–2076.

(7) Li, B.; Wu, L.; Li, L.; Seeger, S.; Zhang, J.; Wang, A. Superwetting double-layer polyester materials for effective removal of both insoluble oils and soluble dyes in water. *ACS Appl. Mater. Interfaces* **2014**, *6*, 11581–11588.

(8) Wang, B.; Liang, W.; Guo, Z.; Liu, W. Biomimetic super-lyophobic and super-lyophilic materials applied for oil/water separation: A new strategy beyond nature. *Chem. Soc. Rev.* **2015**, *44*, 336–361.

(9) Gao, X.; Xu, L. P.; Xue, Z.; Feng, L.; Peng, J.; Wen, Y.; Wang, S.; Zhang, X. Dual-scaled porous nitrocellulose membranes with under-water superoleophobicity for highly efficient oil/water separation. *Adv. Mater.* **2014**, *26*, 1771–1775.

(10) Zouboulis, A.; Avranas, A. Treatment of oil/in-water emulsions by coagulation and dissolved-air flotation. *Colloids Surf., A* **2000**, *172*, 153–161.

(11) Nordvik, A. B.; Simmons, J. L.; Bitting, K. R.; Lewis, A.; Strøm-Kristiansen, T. Oil and water separation in marine oil spill clean-up operations. *Spill Sci. Technol. Bull.* **1996**, *3*, 107–122.

(12) Benner, S. W.; John, V. T.; Hall, C. K. Simulation study of hydrophobically modified chitosan as an oil dispersant additive. *J. Phys. Chem. B* **2015**, *119*, 6979–6990.

(13) Fritt-Rasmussen, J.; Brandvik, P. J. Measuring ignitability for in situ burning of oil spills weathered under Arctic conditions: From laboratory studies to large-scale field experiments. *Mar. Pollut. Bull.* **2011**, *62*, 1780–1785.

(14) Jadhav, S. R.; Vemula, P. K.; Kumar, R.; Raghavan, S. R.; John, G. Sugar-derived phase-selective molecular gelators as model solidifiers for oil spills. *Angew. Chem., Int. Ed.* **2010**, *49*, 7695–7698.

(15) Zhu, Q.; Pan, Q.; Liu, F. Facile removal and collection of oils from water surfaces through superhydrophobic and superoleophilic sponges. *J. Phys. Chem. C* **2011**, *115*, 17464–17470.

(16) Gao, C.; Sun, Z.; Li, K.; Chen, Y.; Cao, Y.; Zhang, S.; Feng, L. Integrated oil separation and water purification by a double-layer TiO<sub>2</sub>-based mesh. *Energy Environ. Sci.* **2013**, *6*, 1147.

(17) Liu, F.; Ma, M.; Zang, D.; Gao, Z.; Wang, C. Fabrication of superhydrophobic/superoleophilic cotton for application in the field of water/oil separation. *Carbohydr. Polym.* **2014**, *103*, 480–487.

(18) Wu, L.; Zhang, J.; Li, B.; Wang, A. Mechanical- and oil/durable superhydrophobic polyester materials for selective oil absorption and oil/water separation. *J. Colloid Interface Sci.* **2014**, *413*, 112–117.

(19) Chen, N.; Pan, Q. Versatile fabrication of ultralight magnetic foams and application for oil–water separation. *ACS Nano* **2013**, *7*, 6875–6883.

(20) Dong, X.; Chen, J.; Ma, Y.; Wang, J.; Chan-Park, M. B.; Liu, X.; Wang, L.; Huang, W.; Chen, P. Superhydrophobic and superoleophilic hybrid foam of graphene and carbon nanotube for selective removal of oils or organic solvents from the surface of water. *Chem. Commun.* **2012**, *48*, 10660–10662.

(21) Wang, G.; Zeng, Z.; Wu, X.; Ren, T.; Han, J.; Xue, Q. Three-dimensional structured sponge with high oil wettability for the clean-up of oil contaminations and separation of oil–water mixtures. *Polym. Chem.* **2014**, *5*, 5942–5948.

(22) Chen, W.; Su, Y.; Zheng, L.; Wang, L.; Jiang, Z. The improved oil/water separation performance of cellulose acetate-graft-polyacrylonitrile membranes. *J. Membr. Sci.* **2009**, *337*, 98–105.

(23) Li, L.; Li, B.; Wu, L.; Zhao, X.; Zhang, J. Magnetic, superhydrophobic and durable silicone sponges and their applications in removal of organic pollutants from water. *Chem. Commun.* **2014**, *50*, 7831–7833.

(24) Du, R.; Gao, X.; Feng, Q.; Zhao, Q.; Li, P.; Deng, S.; Shi, L.; Zhang, J. Microscopic dimensions engineering: Stepwise manipulation of the surface wettability on 3D substrates for oil/water separation. *Adv. Mater.* **2016**, *28*, 936–942.

(25) Gao, X.; Zhou, J.; Du, R.; Xie, Z.; Deng, S.; Liu, R.; Liu, Z.; Zhang, J. Robust superhydrophobic foam: A graphdiyne-based hierarchical architecture for oil/water separation. *Adv. Mater.* **2016**, *28*, 168–173.

(26) Cervin, N. T.; Aulin, C.; Larsson, P. T.; Wågberg, L. Ultra porous nanocellulose aerogels as separation medium for mixtures of oil/water liquids. *Cellulose* **2012**, *19*, 401–410.

(27) Liu, C.; Yang, J.; Tang, Y.; Yin, L.; Tang, H.; Li, C. Versatile fabrication of the magnetic polymer-based graphene foam and applications for oil–water separation. *Colloids Surf., A* **2015**, *468*, 10–16.

(28) Wang, G.; He, Y.; Wang, H.; Zhang, L.; Yu, Q.; Peng, S.; Wu, X.; Ren, T.; Zeng, Z.; Xue, Q. A cellulose sponge with robust superhydrophilicity and under-water superoleophobicity for highly effective oil/water separation. *Green Chem.* **2015**, *17*, 3093–3099.

(29) Zhang, L.; Zhang, Z.; Wang, P. Smart surfaces with switchable superoleophilicity and superoleophobicity in aqueous media: toward controllable oil/water separation. *NPG Asia Mater.* **2012**, *4*, e8.

(30) Zhang, W.; Liu, M.; Liu, Y.; Liu, R.; Wei, F.; Xiao, R.; Liu, H. 3D porous poly(l-lactic acid) foams composed of nanofibers, nanofibrous microsheaves and microspheres and their application in oil–water separation. *J. Mater. Chem. A* **2015**, *3*, 14054–14062.

(31) Liu, S.; Xu, Q.; Latthe, S. S.; Gurav, A. B.; Xing, R. Superhydrophobic/superoleophilic magnetic polyurethane sponge for oil/water separation. *RSC Adv.* **2015**, *5*, 68293–68298.

(32) Grynyov, R.; Bormashenko, E.; Whyman, G.; Bormashenko, Y.; Musin, A.; Pogreb, R.; Starostin, A.; Valtsifer, V.; Strelnikov, V.; Schechter, A.; et al. Superoleophobic surfaces obtained via hierarchical metallic meshes. *Langmuir* **2016**, *32*, 4134–4140.

(33) Darmanin, T.; Tarrade, J.; Celia, E.; Guittard, F. Superoleophobic meshes with high adhesion by electrodeposition of conducting polymer containing short perfluorobutyl chains. *J. Phys. Chem. C* **2014**, *118*, 2052–2057.

(34) Bormashenko, E.; Balter, S.; Bormashenko, Y.; Aurbach, D. Honeycomb structures obtained with breath figures self-assembly allow water/oil separation. *Colloids Surf., A* **2012**, *415*, 394–398.

(35) Li, X. M.; Reinhoudt, D.; Crego-Calama, M. What do we need for a superhydrophobic surface? A review on the recent progress in the preparation of superhydrophobic surfaces. *Chem. Soc. Rev.* **2007**, *36*, 1350–1368.

(36) Chen, Z.; Li, F.; Hao, L.; Chen, A.; Kong, Y. One-step electrodeposition process to fabricate cathodic superhydrophobic surface. *Appl. Surf. Sci.* **2011**, *258*, 1395–1398.

(37) Yang, J.; Zhang, Z.; Men, X.; Xu, X.; Zhu, X. A simple approach to fabricate superoleophobic coatings. *New J. Chem.* **2011**, *35*, 576–580.

(38) Wu, N.; Fu, L.; Su, M.; Aslam, M.; Wong, K. C.; Dravid, V. P. Interaction of fatty acid monolayers with cobalt nanoparticles. *Nano Lett.* **2004**, *4*, 383–386.